TISSUE ENGINEERING: Part A
Volume 21, Numbers 17 and 18, 2015

DOI: 10.1089/ten.tea.2015.0157

termis
Tissue Engineering
& Regenerative Medicine
International Society

ORIGINAL ARTICLE

Functional Reconstruction of Tracheal Defects by Protein-Loaded, Cell-Seeded, Fibrous Constructs in Rabbits

Lindsey M. Ott, PhD,[1] Cindy H. Vu, BS,[2] Ashley L. Farris, BS,[3] Katrina D. Fox, MS, DVM,[4] Richard A. Galbraith, JD, MD, MBA,[5] Mark L. Weiss, PhD,[4] Robert A. Weatherly, MD,[6] and Michael S. Detamore, PhD[1,7]

Tracheal stenosis is a life-threatening disease and current treatments include surgical reconstruction with autologous rib cartilage and the highly complex slide tracheoplasty surgical technique. We propose using a sustainable implant, composed of a tunable, fibrous scaffold with encapsulated chondrogenic growth factor (transforming growth factor-beta3 [TGF-β3]) or seeded allogeneic rabbit bone marrow mesenchymal stromal cells (BMSCs). *In vivo* functionality of these constructs was determined by implanting them in induced tracheal defects in rabbits for 6 or 12 weeks. The scaffolds maintained functional airways in a majority of the cases, with the BMSC-seeded group having an improved survival rate and the Scaffold-only group having a higher occurrence of more patent airways as determined by microcomputed tomography. The BMSC group had a greater accumulation of inflammatory cells over the graft, while also exhibiting normal epithelium, subepithelium, and cartilage formation. Overall, it was concluded that a simple, acellular scaffold is a viable option for tracheal tissue engineering, with the intraoperative addition of cells being an optional variation to the scaffolds.

Introduction

Laryngotracheal disorders resulting in airway obstruction, although rare, can cause significant morbidity and can be life threatening. These disorders are the result of congenital (laryngo/tracheomalacia, congenital subglottic stenosis) or acquired (prolong intubation, traumatic injury, tracheotomy, tumors) causes. The estimated incidence of stenosis in postintubation or tracheotomy patients is 10–20% with only 1–2% being symptomatic or having severe stenosis (estimated 4.9 severe stenosis cases per million per year in the general population).[1,2] Due to the congenital occurrences and increased survival of premature infants requiring prolonged intubation the pediatric population makes up a significant portion of patients requiring treatment.

Treatment options include balloon dilation, laser surgery, stenting, and surgical resection and reconstruction; with reconstruction being the preferred alternative for severe stenosis, though there are limitations to this treatment. Laryngotracheal reconstruction involves augmenting the stenotic region with autologous costal cartilage. A specialized surgical technique and an invasive, multi-site surgery are required for this procedure. Slide tracheoplasty is another surgical treatment option; however, the procedure is highly complex and requires special training. Thus, an off-the-shelf tissue-engineered product is needed that would replace the need for autologous tissue and eliminate the challenges for the surgeon and patient.

Various tissue-engineered trachea replacements exist,[3] including human trials with decellularized donor tissues recellularized with autologous cells,[4,5] nondegradable polypropylene scaffolds coated with natural materials,[6] and a synthetic (polyhedral oligomeric silsesquioxane [POSS] covalently bonded to poly-[carbonate-urea] urethane [PCU]) scaffold designed with the patient computed tomography (CT) dimensions.[7] Allogeneic tracheal tissue was implanted

[1]Bioengineering Program, University of Kansas, Lawrence, Kansas.
[2]School of Medicine, University of Kansas, Kansas City, Kansas.
[3]Department of Molecular Biosciences, University of Kansas, Lawrence, Kansas.
[4]College of Veterinary Medicine, Kansas State University, Manhattan, Kansas.
[5]Anatomic and Clinical Pathology, Lawrence Memorial Hospital, Lawrence, Kansas.
[6]Section of Otolaryngology, Children's Mercy Hospital, Kansas City, Missouri.
[7]Department of Chemical and Petroleum Engineering, University of Kansas, Lawrence, Kansas.

into the trachea, but this procedure required prolonged priming in the forearm before implantation and immunosuppression.[8] Approaches utilizing degradable synthetic materials are gaining popularity due to the limited availability, specialized preparation, and storage of donor tissues, and the limited regenerative capacity of nondegradable materials.[9]

Our approach is unique in that we harness degradable synthetic materials with a biomimetic architecture. We endeavor to use polymeric scaffolds for trachea repair, utilizing electrospun poly(D,L-lactide-co-glycolide) (PLGA) (on outer surface) and polycaprolactone (PCL) (on inner surface) graded scaffolds reinforced with PCL rings for tracheal defect repair. Our hypothesis was that the scaffold would provide an airtight, biocompatible prosthesis with cartilage-like tissue replacement. Our preliminary pilot studies in rabbits indicated that the scaffolds were functional in patch-type tracheal defects (not published). Thus, a larger *in vivo* study was warranted to establish statistically significant efficacy.

Three groups were designed for this study: (1) a gradient scaffold with reinforced rings, (2) a reinforced gradient scaffold with transforming growth factor-beta3 (TGF-β3) encapsulated in the PLGA, and (3) a reinforced gradient scaffold with rabbit bone marrow mesenchymal stromal cells (BMSCs) seeded intraoperatively (Fig. 1). The Scaffold-only group was chosen to determine whether a simple, material-based approach would be adequate as a tracheal construct. The addition of ring supports is crucial for the scaffold integrity and this approach has been used by a few other research groups.[10,11] TGF-β3 was chosen to stimulate cellular growth and healing. BMSCs were added as a common cellular source with potential for chondrogenic differentiation. The objective of this study was to supplement the preclinical data available for tracheal tissue engineering.

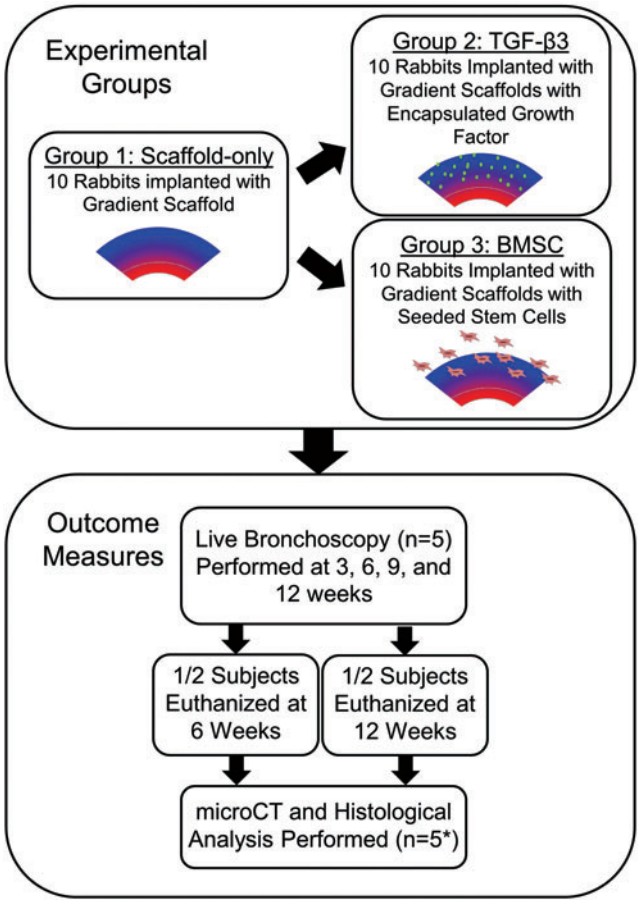

FIG. 1. Overview of the study design. Three groups were tested: Scaffold-only, transforming growth factor-beta3 (TGF-β3), and bone marrow stromal cell (BMSC) seeded (*The actual sample size was reduced due to adverse events [AE] that occurred during the experiment.). Color images available online at www.liebertpub.com/tea

Materials and Methods

Material fabrication

Using a custom-designed electrospinning apparatus, 2 mm thick electrospun fiber sheets were fabricated following a slightly modified protocol established in our previous work.[12] A 7 wt% PCL (inherent viscosity 1.0–1.3 dL/g; LACTEL, Birmingham, AL) solution in 1,1,1,3,3,3-hexafluoro-2-propanol (HFIP; Oakwood Chemical; Columbia, SC) and a 14 wt% poly(D,L-lactide-co-glycolide) copolymer (PLGA, 50:50 lactic acid: glycolic acid, acid end group, MW 50,000 Da, inherent viscosity 0.35 dL/g; Evonik Industries, Birmingham, AL) solution in HFIP were prepared for electrospinning. The solutions were placed in 20 mL syringes and fitted into programmable syringe pumps (PhD Ultra; Harvard Apparatus, Holliston, MA) and set to extrude the solution at 5 mL/h. As the solution was extruded through a charged 20 gauge needle (+10 kV; Glassman High Voltage, High Bridge, NJ), and the charged polymer was drawn from the needle tip to a negatively charged (−6 kV) rotating cylindrical stainless steel mandrel (6.35 mm diameter), with a needle-to-mandrel distance of 20 cm. Safety precautions, personal protective equipment and a well ventilated working environment were used when handling the HFIP solvent.

To create the graded group, 8.33 mL of PCL was first electrospun (0.34 mm layer thickness). PCL rings were then created by mixing 15 w/v% PCL in 1:1 DCM:DMF solution, and pouring the solution into a flat plate and allowing the solvent to evaporate, thus forming a polymer sheet. The PCL strips were cut to 1–2 mm width and had a 1.5 mm thickness. These PCL rings were then affixed with liquid PCL solution to the electrospun PCL and arranged 3–4 mm apart along the length of the cylindrical mandrel. Another 0.34 mm layer of PCL was electrospun over the rings, thus encapsulating the rings between layers. 6.67 mL of PLGA and PCL (total of 13.33 mL total polymer) was then simultaneously electrospun from separate syringes over the PCL layer (0.67 mm layer thickness), followed by 8.33 mL of PLGA electrospun over the PLGA/PCL layer (0.67 mm layer thickness).

To create the protein-loaded PLGA solutions, TGF-β3 (Peprotech, Rocky Hill, NJ) was reconstituted to 1 mg/mL with 10 mM citric acid (251275; Sigma, Milwaukee, WI) and further diluted to 0.8 mg/mL with 0.1% bovine serum albumin (BP9706; Fisher Scientific; Waltham, MA) in sterile phosphate-buffered saline (PBS, P5368; Sigma). The reconstituted protein solutions were individually mixed with the PLGA solutions to reach a final loading ratio of 30 ng of TGF-β3 per 1.0 mg of PLGA (~126 μg of TGF-β3 per scaffold). The final mixtures were then sonicated over ice

(50% amplitude, 20 s). The solutions were electrospun immediately after preparation.

Once the 2 mm wall thickness was achieved, the electrospun tubes were removed from the collecting rod, lyophilized for 24 h, sterilized using ethylene oxide, and aired in a fume hood for 24 h.

Cell source

Bone marrow was harvested from the femurs and tibias of 6- to 8-week-old male New Zealand White rabbits ($n = 3$) under approval from the Institutional Animal Care and Use Committee of the University of Kansas (protocol #175-08). BMSCs were isolated by density gradient centrifugation (Histopaque, 10771; Sigma) and cultured in alpha-MEM (12571; Gibco, Carlsbad, CA), 10% fetal bovine serum (12662; Gibco), and 1% penicillin/streptomycin (15140; Gibco). Cells were passaged to P4 (frozen at P2) before implantation.

Surgical procedure

Animal experiments were approved by the Institutional Animal Care and Use Committee of the University of Kansas Medical Center (protocol #2012–2099). Before the procedure, the rabbit was provided with a warmed saline bolus (60 mL, subcutaneous [SQ]) to ensure proper hydration and to maintain blood pressure. Following the induction of stable general anesthesia (ketamine-100 mg/mL, 30 mg/kg, intramuscular [IM]; xylazine-100 mg/mL, 3 mg/kg, IM; and glycopyrrolate-0.2 mg/mL, 0.01 mg/kg, SQ) and analgesic delivery (buprenorphine-1 mg/mL, 0.1 mg/kg, SQ), hair was shaved from the area around the neck/trachea region of male New Zealand White rabbits (7–8 lbs) ($n = 5$ rabbits/group/end point, 30 rabbits total). Each rabbit was intubated to deliver isoflurane, with the defect being created above the end of the endotracheal tube so that the isoflurane could be reliably delivered. Intubation was assisted with a bronchoscope (10020ATA, Hopkins Telescope, 0°, 2.9 mm, 30 cm; Karl Storz Endoskope; Tuttlingen, Germany) and a video processor coupled to a light source (20045020, TelepackX; Karl Storz Endoskope). Inhaled isoflurane was used to maintain anesthesia. The surgical area was disinfected with alternating scrubs of surgical scrub (povidone scrub or chlorhexidine scrub) and 70% ethanol, and then draped.

A ventral midline cervical incision was made over the trachea, including identification and division of the strap muscles, to access the cervical trachea. Lidocaine (2%)/bupivacaine (0.5%) (up to 3.5 and 4 mg/kg, respectively) was delivered directly to the tracheal defect site or subcutaneously before surgery to alleviate discomfort associated with defect creation. An elliptical defect was marked on the wall of the trachea with an approximate size of 0.5×1.5 cm (with the long axis oriented along the length of the trachea). The defect was centered ~ 2 cm below the cricoid cartilage. The marked area of tracheal wall was removed with sharp dissection using a scalpel, and the resulting defect was patched with a biomaterial scaffold patch (1×2.5 cm) slightly larger than the defect itself to create an airtight seal with ~ 5 mm of overlap around the periphery. The scaffold was cut with surgical scissor in the operating room. Absorbable polydioxanone suture (size 4-0) was used to suture the scaffold to the trachea in all groups. A negative control (unpatched defect) was not possible, as that would have resulted in certain fatality.

In the cell-seeded group, ~ 25 million cells per scaffold were prepared with 7–10% of cells labeled with near-infrared fluorescent quantum dots (Q25071MP; Life Technologies, Carlsbad, CA) for *in vivo* cell imaging and stored in 37°C medium (same composition as for cell culture) in polypropylene tubes until needed for surgery. Cells were collected into polypropylene tubes a few hours before surgery. Before seeding, the cell medium was removed through centrifugation and cells were resuspended in 200 μL of sterile-filtered PBS in the operating room. Once one side of the scaffold was sutured in place, the 200 μL cell slurry was carefully pipetted directly over the entirety of the exterior surface of the scaffold. Cells were allowed to soak for 5 min and then the remainder of the scaffold was sutured in place. Preliminary Trypan blue staining determined that cells remained viable after thawing, transport, and preparation for seeding.

The wound was then closed in layers using running polyglactin 910 suture (3-0 Vicryl; Ethicon, Sommerville, NJ) in the strap muscle layer and the skin closure layer. After each procedure was finished and the rabbit recovered from anesthesia, they were administered meloxicam (5 mg/mL, 0.2 mg/kg, SQ) and returned to their cage once they remained sternal.

Bronchoscopy

A video-endoscopy system consisting of a bronchoscope and video processor, used earlier to assist intubation during the surgical procedure, was used for bronchoscopic evaluation. The degree of re-epithelialization over the scaffold region and appearance of stenotic regions of the trachea were evaluated with a bronchoscope at 3, 6, 9, and 12 weeks after implantation. Procedures were done under anesthesia (ketamine-100 mg/mL, 30 mg/kg, IM; xylazine-100 mg/mL, 3 mg/kg, IM; and glycopyrrolate-0.2 mg/mL, 0.01 mg/kg, SQ) and analgesics (meloxicam-5 mg/mL, 0.2 mg/kg, SQ) were given postprocedure.

Bronchoscopic images were visually assessed and assigned a semi-quantitative score by the following criteria: severity of lumen narrowing (none, slight, moderate, severe), progression of lumen narrowing (none, slight, moderate, severe), direction and type of narrowing (side-to-side, graft collapse, swelling), and re-epithelialization of the graft (none, slight, moderate, complete).

In vivo *imaging*

A preclinical *in vivo* fluorescence imaging system (IVIS Spectrum; PerkinElmer, Waltham, MA) was used to detect the quantum dot-labeled cells. *In vivo* cell tracking was planned at 3, 6, 9, and 12 weeks postoperation. Briefly, the subjects were anesthetized (as described for bronchoscopy) and positioned in the imaging system to visualize the neck region. The system was set to sweep at excitations of 400, 450, and 550 nm and emission collection at 480 and 820 nm. Fluorescence could not be detected through the animal's skin and muscle (data not shown). Further cell tracking was not pursued during this study and no postexplant imaging was explored because fluorescent emission would likely be quenched by 6 weeks. Future cell tracking should be

conducted with other imaging techniques, such as magnetic resonance imaging.

microCT acquisition

At 6 and 12 week end points, tracheas were excised and fixed in 10% neutral buffered formalin. To aid in soft tissue visualization in the microCT analysis, the fixed tracheas were soaked in 40% Hexabrix (Mallinckrodt, St. Louis, MO)/60% PBS for 10 h.[13] All tracheas were secured in a vertical position during scanning. To prevent dehydration during scanning, the tracheas were placed in a sealed tube. All scans were performed using a 3D X-ray imaging system (Xradia MicroXCT-400, Pleasanton, CA) at 40 kV, 8 W, 2–4 s exposure time, and 0.5× objective magnification. For high quality images, 1600 projections were collected with multi reference images selected at 10 images every 400 frames for a total acquisition time of 2.5–5 h. After acquisition, the images were manually reconstructed using the Xradia software where several files were generated including an AmiraMesh file. The center shift and beam hardening were determined.

microCT analysis

Following microCT reconstruction, the AmiraMesh files were processed in the Avizo Fire software (FEI Company, Hillsboro, OR) to quantify luminal volume. Within the Avizo Fire software, a modified pore quantification procedure was used to quantify the lumen volume. Briefly, the AmiraMesh file was trimmed to only contain the length of trachea containing the scaffold. This was determined by manually viewing the transverse CT slices and visualizing the proximal and distal edge of the scaffold. To obtain the void space, interactive thresholding was applied to define the void space in the CT image and a binary image file was created. The quantification command ''I_Analyze'' was used to obtain quantitative data (volume, area, length) for each void space. The image was then filtered based on volume, resulting in the isolation of the lumen void space from other void space in the image. Once the lumen space was isolated, the volume and length of the 3D image and max/min area of the 2D slices were recorded for statistical analysis. To account for variation in trachea length measured in the software (mean length = 2.51 ± 0.15 cm), the length was divided by the lumen volume creating an ''average cross-sectional area'' in cross-sectional area units. To obtain a ''native trachea'' average cross-sectional area measurement, the healthy, unaltered regions of the tracheas were quantified.

Histological analysis

Following microCT analysis, the tracheas were soaked in PBS for 24 h to remove contrast agent and then placed in formalin. The samples were dehydrated in graded ethanol and paraffin embedded. Transverse sections were taken on a Microm HM 355S microtome (Thermo Scientific, Waltham, MA) using a low-profile disposable blade (3052835; Thermo Scientific) with a sample thickness of 5 μm. Sections were placed on positively charged slides, heated to 60°C for 1 min, and allowed to dry at room temperature overnight. Before staining, the slides were heated to 60°C for 45 min. After drying, the paraffin was removed from the slides and the tissue was rehydrated using CitriSolv (22143975; Fisher Scientific) and a graded series of ethanols.

Hematoxylin and Eosin (H&E) staining for cell nuclei and general tissue visualization was performed using the following protocol. Slides were stained with Harris Hematoxylin (SH30-4D; Fisher Scientific) for 3 min, rinsed with water, dipped in acid ethanol, rinsed in water, and stained with Eosin Y (119830-25g; Sigma-Aldrich, St. Louis, MO) for 30 s. Safranin-O/Fast Green staining for glycosaminoglycans (GAGs) was performed using the following protocol. Slides were stained with Harris Hematoxylin (SH30-4D; Fisher Scientific) for 3 min, rinsed with water, dipped in acid ethanol, rinsed with water, stained in Fast Green (F7258; Sigma-Aldrich) for 3 min, dipped in 1% acetic acid (537020; Sigma-Aldrich), stained in 0.1% Safranin-O (S8884; Sigma-Aldrich) for 10 min, and rinsed with water. Alcian Blue staining for GAGs was performed using the following protocol. Slides were stained with Alcian Blue solution (A3157; Sigma-Aldrich) for 30 min, rinsed in water, stained with Nuclear Fast Red solution (IW-3021; IHC World, Woodstock, MD), and rinsed with water. Verhoeff-Van Gieson staining for collagen and elastin was performed using the following protocol. Slides were stained with Verhoeff's solution (hematoxylin-ferric chloride-iodine solution) (H9627, 157740, 207772, 221945; Sigma-Aldrich) for 1 h, rinsed with water, dipped in 2% ferric chloride (157740; Sigma-Aldrich) for 2 min, rinsed with water, dipped in 5% sodium thiosulfate (S7026; Sigma-Aldrich) for 1 min, rinsed in water, and stained in Van Gieson's solution (1% aqueous acid fuschin in picric acid) (F8129, Sigma-Aldrich; 80456, Fluka, Buchs, Switzerland) for 5 min. Sudan Black B for residual polymer was performed according to manufacturer's instructions (IW-3021; IHC World).

All sections were then dehydrated in graded ethanol and then cleared in Citrisolv and mounted, with the exception of Sudan Black, where the sections remained hydrated and were mounted with aqueous mounting medium (E01-15; IHC World). Photomicrographs were taken of representative sections.

Histological scoring

The histological sections were scored blind by a pathologist (R.A.G.). The scoring system was developed to evaluate inflammation, vascularization, epithelialization, cartilage formation, and residual polymer. The location of inflammation was determined by the spatial organization of inflammatory cells/tissue (i.e., diffuse or on outer surface of scaffold) and severity of inflammation was determined by the thickness of the ''cap'' like tissue on the exterior surface of the scaffold. Inflammatory cell types were differentiated and quantified into multi-nucleated giant cells (MNG cells), mononuclear cells (e.g., macrophages, lymphocytes, plasma cells), heterophils (i.e., rabbit analog of neutrophils),[14] and eosinophils. To determine vasculature, four representative fields of inflamed tissue were examined at 40× (Axio Imager A1 Microscope; Carl Zeiss Microscopy, Thornwood, NY) and vessel cross sections containing erythrocytes were counted.

Epithelialization was analyzed by simply categorizing it into two groups—presence or absence of epithelium (yes or no). The epithelial character was further described and

categorized into pseudostratified columnar, simple cuboidal, stratified cuboidal, simple columnar, squamous, and ulcer formation. Subepithelial character was described as fibrous, vascular, inflamed, or a combination. Cartilage formation was assessed by detecting new or immature cartilage and by assessing collagen staining (Verhoeff-Van Gieson) and collagen location. The presence of fibroblasts and their locations were also noted. The amount of polymer present from the Sudan Black staining was ranked from no polymer (0), 25% (1), 50% (2), 75% (3), and 100% of polymer present (4).

Statistical analysis

Using one-way ANOVA and Tukey's *post hoc* analysis, the bronchoscopy rating, lumen average cross-sectional area, and histological scoring were determined to be significant if $p < 0.05$ (IBM SPSS, Armonk, NY).

Results

Mortality

The implantation of the scaffolds was straightforward, with the scaffolds being easily cut into the desired elliptical shape in the operating room and sutured into the induced defect (Fig. 2). Throughout the 6 or 12 weeks of study, a majority of the rabbits (22 subjects) did not display any signs of distress. In the event of an adverse reaction (e.g., labored breathing, coughing, weight loss, stridor), the rabbit underwent bronchoscopic evaluation, vital sign monitoring, and more frequent monitoring. If the animal's condition was rapidly declining and no intervention methods were available, euthanasia was determined to be the most appropriate course of action. Adverse events occurred in eight of the 30 subjects (27%), with a breakdown of three subjects in the scaffold-only group (one subject from the 6 week group and two subjects from 12 week group), four subjects in the TGF-β3 group (two subjects from the 6 week group and two subjects from the 12 week group), and one subject in the BMSC group (from the 6 week group) (Fig. 3).

Bronchoscopy

The purpose of the bronchoscopic analysis was to reveal the real-time morphology of the airway through the course of the study (Fig. 4). Severity of stenosis was rated on a scale of no stenosis (0), slight (1), moderate (2), to severe (3). In the overall population, 34% of subjects exhibited no to slight stenosis and 66% exhibited moderate to severe stenosis. In the survival cases (no adverse events), 34% of subjects exhibited no to slight stenosis and 45% exhibited moderate to severe stenosis (remaining 21% were adverse events). The adverse events all exhibited the most severe level of stenosis, although no statistical analysis could be done due to do the small number of adverse events (Fig. 5). Of the cases exhibiting slight to severe stenosis, the progression of the stenosis over time was evaluated on a scale from no change (0), slight (1), moderate (2), to severe (3). Similar to the stenosis severity rating, we observed that the 12 week subjects exhibited a severe progression of stenosis as compared to the 6 week subjects (not statistically significant).

Re-epithelialization was assessed on a scale from none (0), slight (1), to moderate (2). All of the subjects exhibited

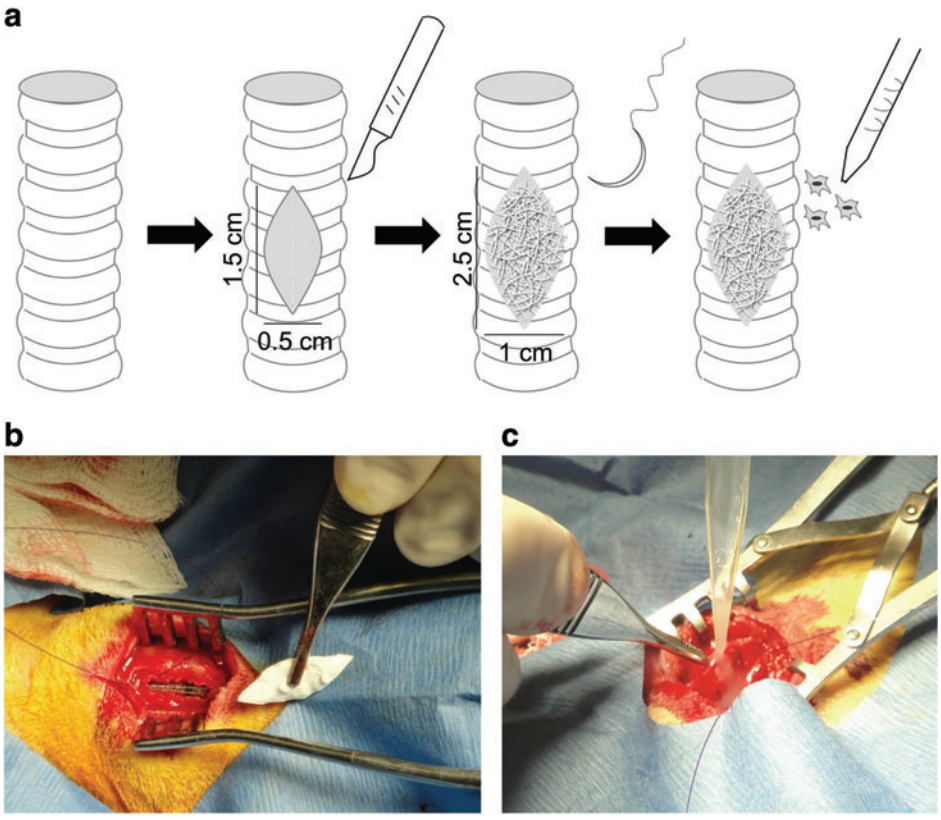

FIG. 2. Surgical schematic of defect creation and scaffold implantation **(a)**. Photographs of the surgical procedure showing induced tracheal defect and placement of scaffold **(b)** and intraoperative cell seeding **(c)**. Color images available online at www.liebertpub.com/tea

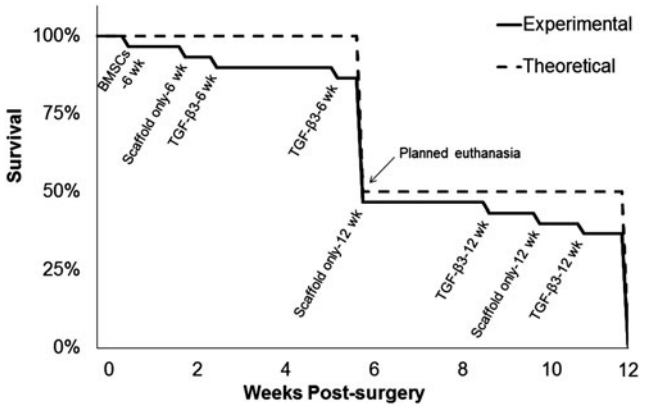

FIG. 3. Chart mapping the survival rate of subjects over the course of 12 weeks.

some degree of epithelialization over the implant area with no statistically significant trends observed. Trends of note include, the degree of epithelialization declined by 50% over time in the TGF-β3 subjects, where a moderate degree of epithelialization was observed at week 6 and a slight degree of epithelialization was observed at week 12 (not statistically significant). The Scaffold-only and BMSC groups did not exhibit the same decreasing trend from 6 to 12 weeks, as the TGF-β3 group. At 6 weeks, the TGF-β3 and BMSC subjects had a 33% higher degree of epithelialization than the Scaffold-only subjects (not statistically significant). The fatal cases appeared to have a lesser degree of epithelialization, all scoring at slight epithelialization (not statistically significant).

The types of stenosis (of the stenotic cases) were categorized into side-to-side narrowing, in-folding of one of the tracheal walls, and scaffold displacement into the airway. It is important to note that no granulation tissue (obvious protrusion of granular tissue) was observed on the lumen surface of any of the implants, indicating that inflammatory tissue overgrowth occluding the airway was not the type of stenosis observed. A large majority of the stenosis subjects exhibited a side-to-side narrowing (84% of total subjects with stenosis), with fewer subjects exhibiting one-wall in-folding (8% of total subjects with stenosis) and scaffold obstructing airway (8% of total subjects with stenosis). The two cases of scaffold obstruction occurred in the Scaffold-only group and the two cases of one-wall in-folding occurred in the Scaffold-only and BMSC group.

In summary, bronchoscopy data indicated 66% of all subjects exhibited moderate to severe stenosis, fatality was linked to stenosis, epithelium was present in all groups, and side-to-side in-folding of tracheal walls was the dominate type of stenosis.

MicroCT and average cross-sectional area quantification

Visual inspection of the microCT scans revealed that all of the groups had some degree of stenosis as compared to a native, unaltered trachea. Analysis with specialized imaging software provided quantitative lumen average cross-sectional area data (Fig. 6).

Average cross-sectional area quantification indicated that the Scaffold-only and TGF-β3 groups maintained an average cross-sectional area similar to the healthy portions of implanted trachea or the ''native trachea'' at both 6 and 12 weeks (i.e., no statistically significant differences). In contrast, the adverse events (fatalities) in the Scaffold-only and TGF-β3 groups had a 33–35% reduced average cross-sectional area compared with the native tracheas ($p < 0.05$). The BMSC group at weeks 6 and 12 had a 27–28% smaller average cross-sectional area ($p < 0.05$) than the native tracheas (Fig. 7).

Within the Scaffold-only group, the surviving week 12 subjects had a lumen average cross-sectional area that was

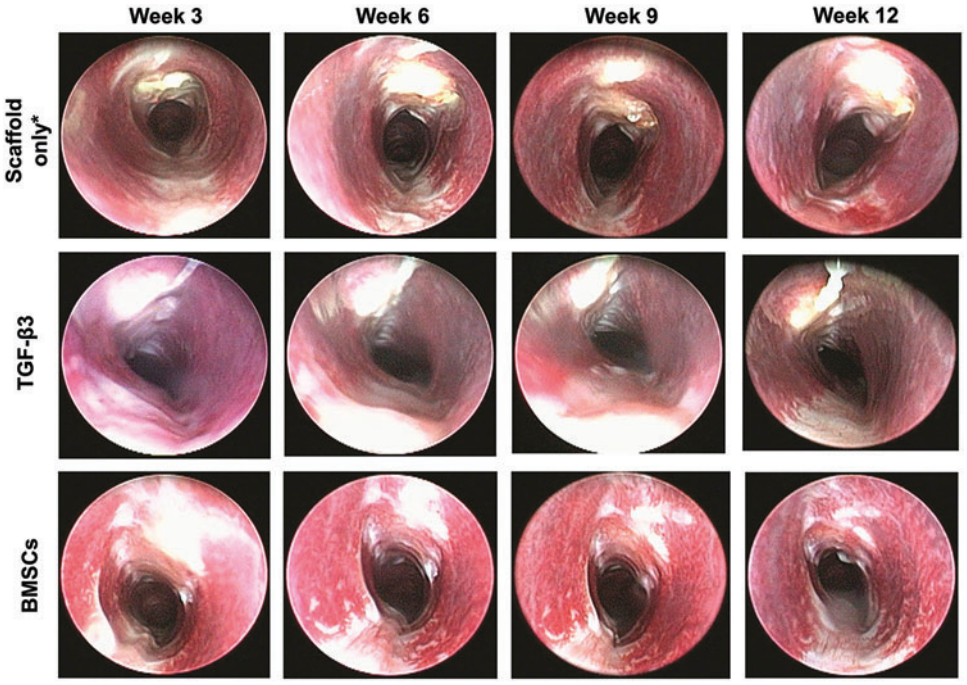

FIG. 4. Representative bronchoscopic images from each experimental group at the four bronchoscopy time points (3, 6, 9, and 12 weeks). The most common type of stenosis observed was side-to-side narrowing that occurred in 84% of total subjects with stenosis. Note that the photograph orientation is such that the scaffold is at the *top* of the photograph in each panel. *Bronchoscopy in the Scaffold only group was performed at week 7 and 10, instead of week 6 and 9. Color images available online at www.liebertpub.com/tea

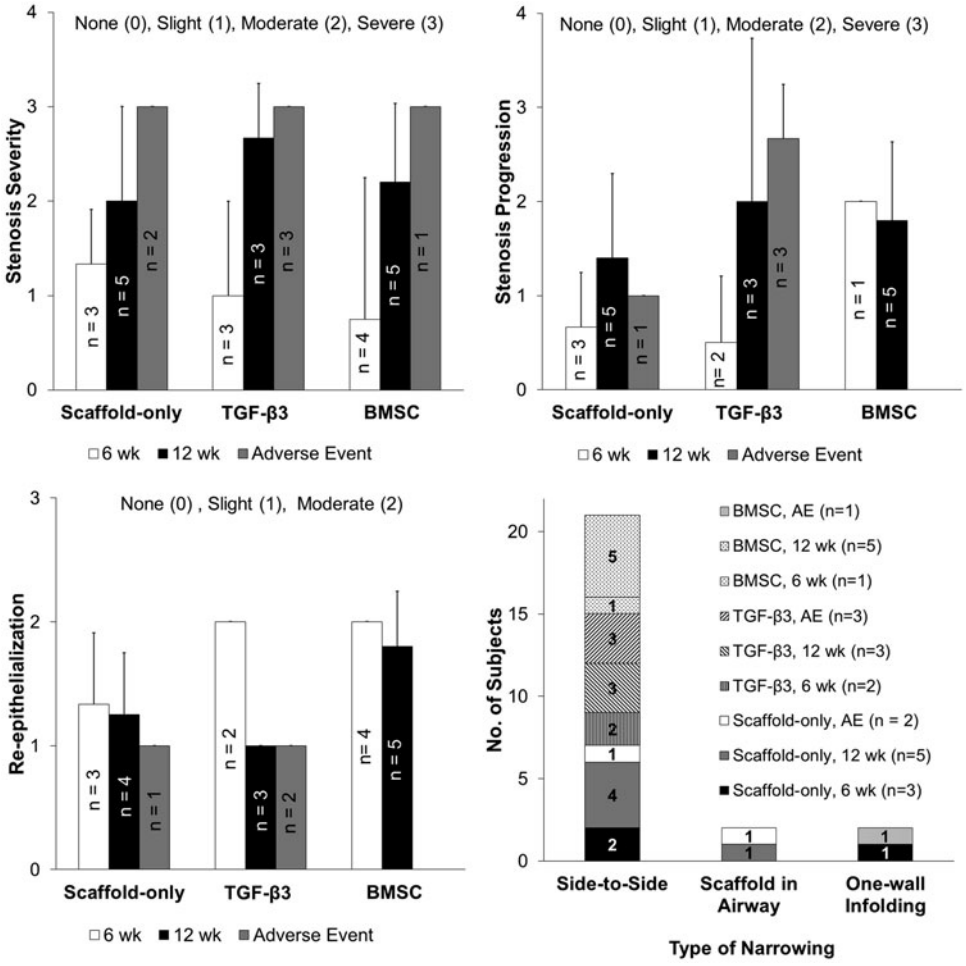

FIG. 5. Bronchoscopy image scoring based on stenosis severity, stenosis progression, type of stenosis, and re-epithelialization (no statistically significant differences).

29% larger than the adverse events ($p < 0.05$). For the Scaffold-only group, the average cross-sectional area corresponding to fatality was $0.19 \pm 0.02\,cm^2$. Among groups, the only statistically significant difference was that the Scaffold-only subjects had a 24% larger average cross-sectional area than the BMSC subjects at week 12 ($p < 0.05$).

In addition, the 2D microCT slice data were analyzed (data not shown) and the location (cranial, middle, caudal) of the narrowest region of the trachea were summarized. The point of greatest stenosis occurred exclusively at the midpoint of the implants (data not shown). Future work could include an in-depth analysis of the 2D data along the trachea length. Kiesler *et al.*[15] mapped the area data in a line graph to convey the length and degree of stenosis.

In summary, CT quantification data indicated that the BMSC group and adverse events in all groups had significantly

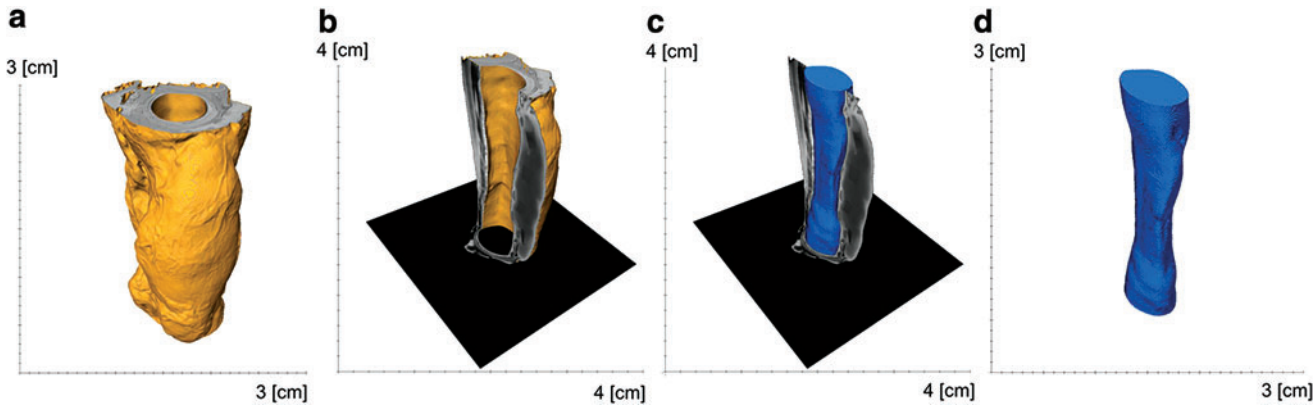

FIG. 6. Illustration of the lumen quantification process in Avizo Fire. The computed tomography data were rendered into a 3D volume (trachea in *yellow*) **(a)**. The lumen space was thresholded and reconstructed into a 3D volume and quantified (lumen in *blue*) **(b–d)**. Color images available online at www.liebertpub.com/tea

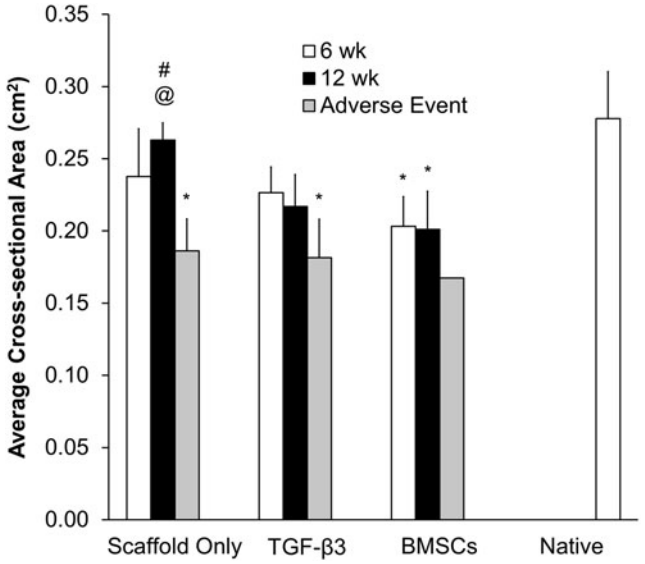

FIG. 7. The average cross-sectional area statistics from the Avizo Fire quantification. The volume was normalized to the trachea length (volume divided by length). The sample sizes in each group and time point were the following: Scaffold-only 6 week ($n=3$), Scaffold-only 12 week ($n=4$), Scaffold-only AE ($n=2$); TGF-β3 6 week ($n=3$), TGF-β3 12 week ($n=3$), TGF-β3 AE ($n=3$); BMSC 6 week ($n=4$), BMSC 12 week ($n=5$), BMSC AE ($n=1$). The BMSC group was the only group to have significantly smaller average cross-sectional area than the native tracheas, aside from the AE (# significantly larger average cross-sectional area when compared to the AE in the same group [$p<0.05$], @ significantly larger average cross-sectional area when compared to the BMSC-group at week 12 [$p<0.05$], * significantly smaller average cross-sectional area when compared to the native tracheas [$p<0.05$]).

smaller airways than the native tracheas, while the Scaffold-only and TGF-β3 subjects had average cross-sectional areas similar to the native tracheas. Adverse event subjects had smaller lumen average cross-sectional areas, indicating there could be a stenosis threshold associated with fatality. The Scaffold-only group had larger tracheal average cross-sectional areas, and thus less stenosis, than the BMSC group. And finally, the narrowest region of the tracheas occurred exclusively at the midpoint of the scaffold length.

Histology

A representative overview of histological sections stained with H&E, Alcian Blue, Safranin O, Verhoeff-Van Gieson, and Sudan Black is provided in Fig. 8. Regions of immature cartilage formation were observed at defect edges and over the defect (in two cases) (Fig. 9). Generally speaking, immature cartilage has a higher density of cells, and the matrix is bluer with H&E than in mature cartilage, which is a reflection of the lower collagen fiber density compared to mature cartilage. Scaffold-only subjects had three cases of immature cartilage formation, with two cases at 6 weeks and one case at 12 weeks. TGF-β3 subjects also had three cases, with two occurring at 12 weeks and one occurring in an adverse event case. The cell-seeded group had six instances of new cartilage formation, occurring mainly at 12 weeks (four cases).

Fibroblasts were observed in all subjects, usually oriented in a layer around the scaffold, between scaffold layers, and in the subepithelium. Unique fibrous, connective tissue was observed inside the scaffold in the 6 week BMSC cases located inside the scaffold (Fig. 9). Collagen was moderately present, with no particular differences among groups, and was located in regions similar to the fibroblasts (Figs. 9 and 10).

Though no statistically significant differences were observed from residual polymer assessment, there was a decreasing amount of polymer remaining over time and the BMSC group had less polymer present compared with the other groups (Fig. 10).

Macroscopic assessment of inflammatory cells involved evaluating thickness (i.e., linked to severity) and location of the inflammatory cell-containing region (Figs. 8 and 9). Inflammatory cells were mainly located on the outer layer of the scaffold (i.e., opposite the luminal side), forming a ''cap'' over the scaffold. Diffuse distribution of inflammatory cells was only observed in two subjects (i.e., adverse events with Scaffold-only and TGF-β3). BMSC-seeded scaffolds at week 12 had more severe inflammation (i.e., a thicker layer of inflammatory tissue) than the Scaffold-only group at week 6 ($p<0.05$) (Fig. 11). Overall there was a trend of increasing severity over time and in the adverse events (Fig. 9).

Microscopic assessment of inflammatory cell types showed that MNG cells were severely present in all groups, except for a few adverse event cases (Figs. 9 and 11). Mononuclear cells were also moderately to severely present in all groups. Heterophils were moderately present. Eosinophils were not present except for a single case in the Scaffold-only group and a single case in the BMSC group (Fig. 9).

The quantification of blood vessels showed that the TGF-β3 group at week 6 had a significantly higher quantity of vasculature than any other group including adverse events ($p<0.05$) (Fig. 11). It appeared that the TGF-β3 treatment increased vasculature at the early time point but the vasculature declined, but did not diminish completely by the later time point ($p\leq 0.05$). Adverse events in the Scaffold-only and TGF-β3 groups had more vasculature than in nonfatal cases in the Scaffold-only and TGF-β3 groups, respectively ($p<0.05$).

Epithelium assessment revealed that all scaffolds had epithelium present, except for five adverse event cases. Different types of epithelium were present. Epithelium was ciliated to some degree in subjects with epithelium. Pseudostratified columnar epithelium was the most common epithelium, with 21 subjects exhibiting this morphology. Of the 21 cases, most subjects exclusively exhibited pseudostratified columnar epithelium while six subjects had a combination of other types of epithelium—cuboidal, simple cuboidal, stratified cuboidal, and simple columnar. A majority of the pure pseudostratified columnar cases were from the BMSC group (seven cases) or the week 12 cases in all groups (nine cases). The simpler epithelium (i.e., simple columnar, cuboidal, and squamous types) was observed in five cases, all of them at the 6 week end point, and those cases were spread across all three treatment groups. Ulcers were observed in the adverse events subjects (three cases), indicating that granulation tissue was present in the airway, which could not be determined with bronchoscopy. Interestingly, subjects with no or poor quality epithelium

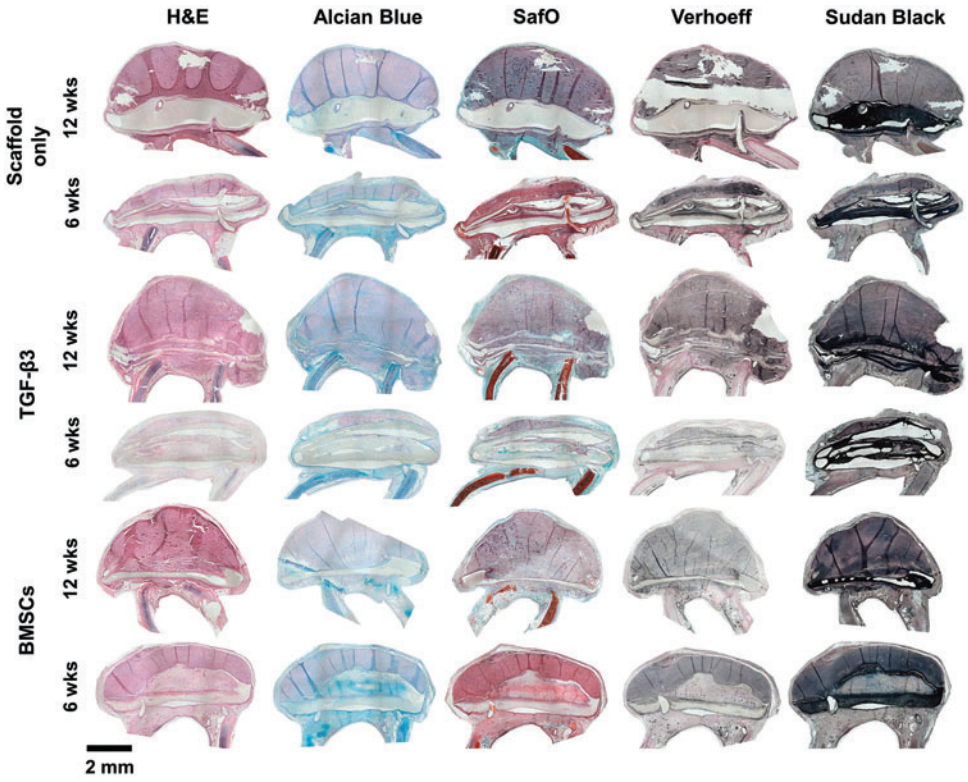

FIG. 8. An overview of histological images in all three groups at the two time points. Hematoxylin and Eosin (H&E), Alcian Blue, Safranin O, Verhoeff-Van Gieson, and Sudan Black staining was performed. Normal epithelium (i.e., pseudostratified columnar) was present more often in the BMSC groups and at later time points. Immature cartilage was observed across all groups, but with a higher occurrence in the BMSC group. Fibroblasts and collagen were present in all subjects, mainly organizing around the scaffolds and within the scaffold. Normal connective fibroblastic tissue was observed inside the BMSC group scaffolds. Transverse sections are oriented with the scaffolded region at the *top* of the image and remaining native trachea rings at the *bottom* of the section (entire circumference of trachea section omitted due to space constraints). Scale bar represents 2 mm. Color images available online at www.liebertpub.com/tea

(ulcerous) were all adverse event cases, making up over half of the adverse events (five of eight cases). Distribution of these cases were relatively even across the treatment groups (two Scaffold-only subjects, two TGF-β3 subjects, and one BMSC group).

The subepithelium was assessed for its vascular and fibrous nature. Inflammation was also noted. A large majority of subjects had a fibrous character (10 purely fibrous and 16 in combination with vascular and/or inflamed tissue). BMSC-seeded scaffolds made up the majority of fibrovascular subepithelium (six of nine cases). Subepithelial vasculature was observed in 13 cases and inflammation was observed in seven cases. The Scaffold-only subjects did not have any occurrence of inflamed subepithelium, while adverse event cases usually had inflamed subepithelium (six of eight cases).

In summary, the outer surface of the scaffold was covered by a layer of inflammatory cells, with a thicker layer of these cells occurring in the BMSC group than in the Scaffold-only group. The inflammatory cells present, as determined with H&E staining, were MNG cells, mononuclear cells, and heterophils. The degree of vascularization was higher in the TGF-β3 group when compared to the other groups, but the vasculature diminished by 12 weeks. Normal epithelium (i.e., pseudostratified columnar) presented more often in the BMSC groups and at later time points. Fibrovascular subepithelium occurred more often in the BMSC groups, while the Scaffold-only group had no incidences of inflamed subepithelium. Immature cartilage was observed across all groups, but with a higher occurrence in the BMSC group. Fibroblasts and collagen were present in all subjects, mainly organizing around the scaffolds and within the scaffold. Normal connective fibroblastic tissue was observed inside the BMSC group scaffolds.

Discussion

This was the first study to evaluate an off-the-shelf fibrous scaffold for patch-type tracheal defects, which are clinically relevant for a larger patient population than entire segmental defect replacements. We also considered the benefits of adding a GF or cells to the tracheal scaffolds. There are two primary requirements for a successful tracheal implant, first, mechanical integrity to maintain airway patency, and second, epithelium coverage over the luminal surface.[16] Without epithelium, constructs can be susceptible to bacterial invasion, granulation tissue formation, and restenosis.[17]

We observed that severe stenosis from scored bronchoscopy images did not consistently result in fatality. Of the bronchoscopy images scored as severe, approximately half

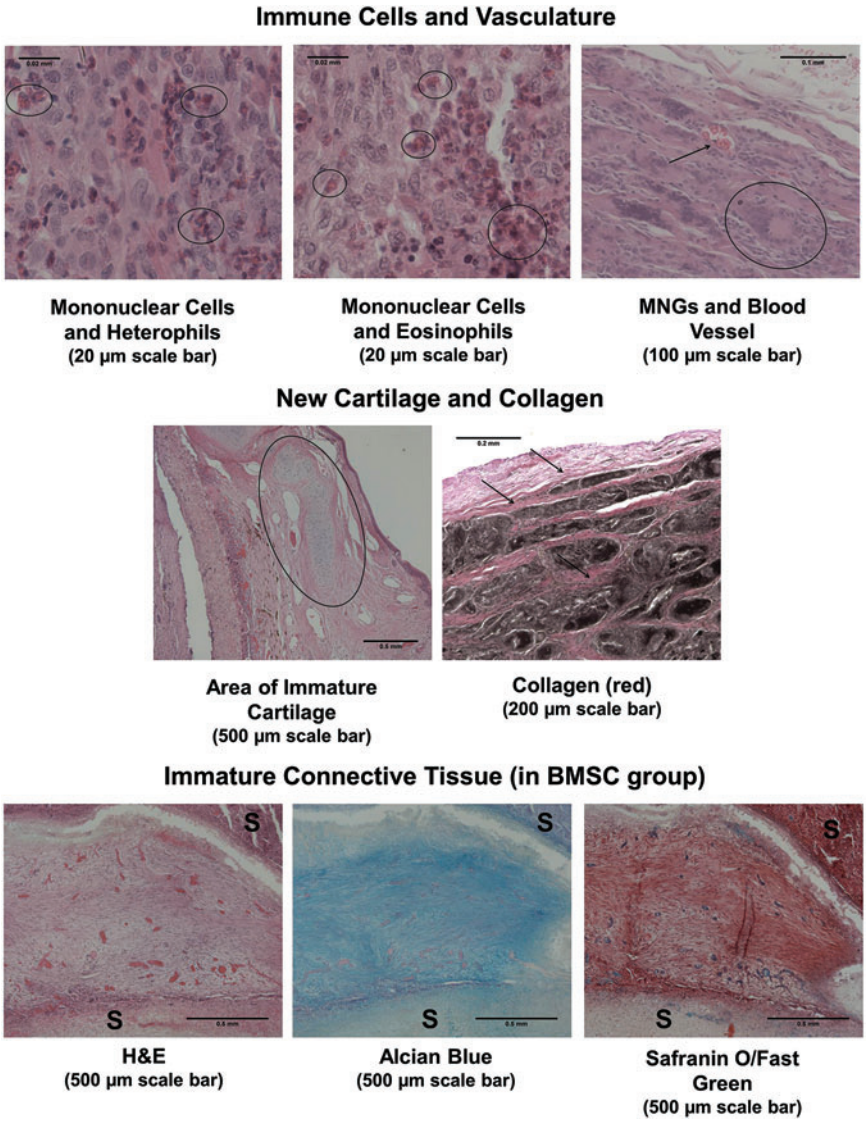

FIG. 9. Magnified histological images representing scoring criteria. Representative images demonstrate the appearance of mononuclear cells, heterophils, eosinophils, multi-nucleated giant cells (MNGs), and vasculature. Regions of immature cartilage and collagen are shown. The unique immature connective tissue is shown in three stains and is surrounded by the scaffold (S). Color images available online at www.liebertpub.com/tea

were fatal. Severe stenosis appears to be necessary for fatality, but does not necessarily lead to fatality. We observed that the predominant type of stenosis was tracheal wall deformation and migration of the native trachea wall into the laryngofissure, not graft dislodgement occluding the airway. This wall deformation could be due to (1) the scaffold weakness and inability for construct to adequately support the surrounding tissue, (2) inflammatory response, or (3) the innate fragility of the rabbit trachea wall that is compounded by the defect creation.

The microCT lumen quantification data suggested that the TGF-β3 group and the Scaffold-only group had significant lumen average cross-sectional areas, both similar to the native tracheas. In addition, the Scaffold-only group had a greater lumen average cross-sectional area as compared to the BMSC-seeded group. The native trachea-like performance of the Scaffold-only group and TGF-β3 group supports an acellular approach as a viable option for trachea defect repair.

An assessment of the cellular response to the constructs revealed that acute inflammatory cells (e.g., heterophils) and chronic inflammatory cells (e.g., mononuclear, MNG cells) were present in all cases. Since tissue was collected 6 and 12 weeks postimplantation, the later stages of the inflammation response were captured with histology, in which a smaller population of heterophils and larger population of mononuclear and MNG cells were present.[18] In the fatality cases, the inverse was observed with higher populations of neutrophils and lower populations of MNG cells. The inverse cell profile in fatal and nonfatal cases indicates that fatal cases had an acute inflammatory reaction, which could be a result of (1) the histology capturing early inflammation due to the adverse events occurring soon after implantation or (2) the host cells could not transition to chronic inflammation with potential for healing. No clear trend in cell types was observed among groups, except that the inflammation severity (thickness of inflammatory cell layer) was higher in the BMSC group than other groups. Although inflammatory response severity occurred in the BMSC group, survival was the highest in this group. Thickness of accumulated inflammatory cells over the implant may not be linked to survival, although this indicates a heightened inflammatory response.

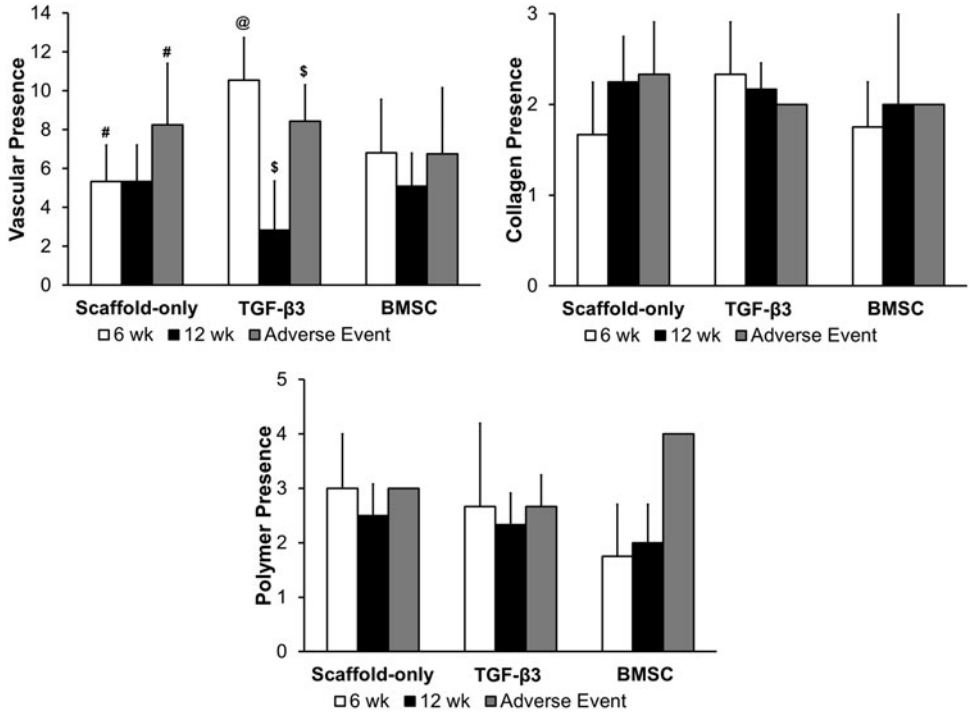

FIG. 10. Histological scoring of vasculature, collagen, and residual polymer. To determine vasculature, four representative fields of inflamed tissue were examined at 40× and vessel cross sections containing erythrocytes were counted. Collagen was scored by assessing if no collagen was present (1), few collagen fibrils present (2), and many collagen fibrils present (3). The amount of polymer present was ranked from no polymer (0), 25% (1), 50% (2), 75% (3), and 100% of polymer present (4) (@ significantly higher quantity of vasculature than other groups [and AE] within the TGF-β3 group [$p < 0.05$], # and $ significantly higher quantity of vasculature than nonfatal cases within their respective groups [$p < 0.05$]).

It is unlikely that the acellular implants generated a response analogous to acute allograft rejection, although it is possible that the MNG cells observed in the BMSC group may have indicated an immune response to the cells similar to rejection in addition to the foreign body reaction. Such a ''rejection'' response would be primarily T lymphocytes, which would fall under the mononuclear group that was assessed, and the target of such lymphocytes would be the transplanted BMSCs. For this reason, we emphasize that an analogous cellular approach in the clinic would be best served by a patient's autologous BMSCs rather than risk immunogenicity from a BMSC donor.

Immature cartilage was observed in all groups, but more often in the BMSC group. This could indicate that the cartilage is either an artifact of the histology section or the BMSCs contributed to cartilage formation.[19] Less residual polymer was present in the BMSC group, indicating that the addition of cells could accelerate degradation, which could

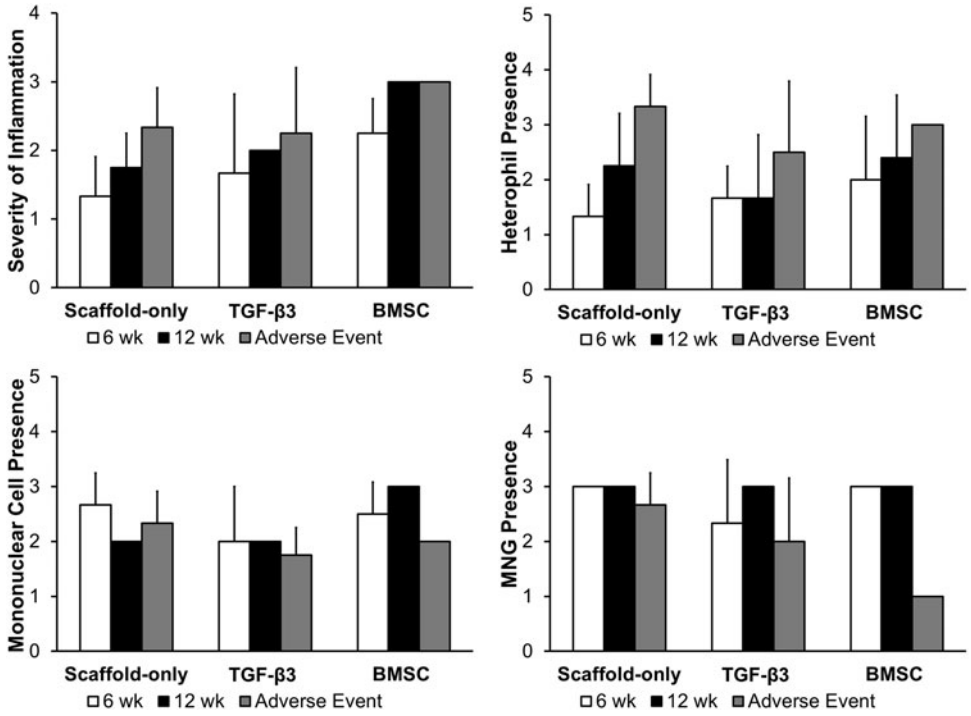

FIG. 11. Histology scoring of inflammatory component of tissue sections. Severity of inflammation across entire section was determined, and scoring of specific inflammatory cell types, including heterophils, mononuclear cells, and MNGs.

be potentially related to increase phagocytosis of polymer material by inflammatory cells.

The bronchoscopy rating of epithelial coverage indicated that all subjects had some degree of epithelium. However, histology is more informative for epithelium quantification. Lack of epithelium was linked to adverse event cases. The reason why epithelium may not have formed on the scaffold could be (1) variable response from subject to subject or (2) that the scaffold was not implanted in such a way to ensure an adequate interface with native tracheas for epithelial migration. Additionally, the later time point subjects had a higher occurrence of normal epithelium indicating that more complex epithelium takes time to migrate and develop on the scaffold lumen.[17] In future studies, immunohistochemical analyses may facilitate in discerning tissue neogenesis versus adjacent mucosa ingrowth.

Histology was also used to assess the degree of vascularity and an increase in vasculature in the TGF-β3 group was observed. Vasculature was observed in all subjects, and the TGF-β3 treatment increased vasculature at early time points but the vasculature declined at later time points, which was expected as TGF-B3 has been known to induce angiogenesis.[20] Angiogenesis occurs in granulation tissue and the normal healing process.

Seeded cells have been shown to have an indirect role in graft development through modulation of the host cell behavior. Harrington *et al.*[21] provided one such example, where they found that seeded macrophages migrated away from a tissue-engineered vascular graft soon after implantation. The same scenario could be true for the tissue-engineered trachea, in which case the BMSCs seeded onto our scaffolds may have promoted a host cell response. Thus, the cells observed in histology are most likely host cells.

Maintaining the bioactivity of the encapsulated TGF-β3 is crucial, as fabrication and solvents may denature proteins. As noted above, the TGF-β3 containing scaffolds had a statistically significant increase in vasculature compared to growth factor-free scaffolds at week 6, indicating a distinct response to TGF-β3 incorporation. Protein release quantification and bioactivity testing should be conducted as a follow-on study, but previous studies in our group[22] and other groups[23,24] have indicated that proteins maintained some activity and induced a cellular response after release from scaffolds, though various techniques such as coaxial electrospinning, salt complexation, hydrophilic additives, and pH-maintaining basic salt additives can be used to improve protein stability.[24,25]

Factors to account for in the data interpretation include the difference between the bronchoscopy rating and the CT lumen quantification could occur because (1) of the subjective nature of the bronchoscopy rating, (2) the lumen quantification's ability to account for the length of stenosis, which can be difficult to determine from the 2D fixed view of the bronchoscopic images, and (3) tissue distortion occurring during the excision and fixation processes. Furthermore, the airway is dynamic, so the lumen can change shape and size based on inspiration and expiration. These static testing methods, such as microCT, only evaluate the trachea dimensions at one morphology. If live CT methods are employed in the future, four-dimensional dynamic volume multidetector computed tomography (4D-CT) could be used to account for variation in airway diameter.

Given our unpublished pilot studies, where 100% survival was observed with eight rabbits at end points up to 6–7 weeks, and which gave us confidence to proceed with this study, we did not anticipate the fatalities observed in the current study. Therefore, we closely considered experimental variations between the pilot studies and the current large-scale study. The variations between the pilot and large experiments were (1) change in electrospinning solvent from dichloromethane (DCM) to HFIP, (2) variable electrospinning parameters that affected scaffold thickness and morphology, (3) animal size changed from 8 to 9 lb in pilot study to 7–8 lb animals in large study, and (4) possible variation in surgical technique. The solvent change is unlikely, as any residual solvent should be removed as the scaffolds are lyophilized and aired in a fume hood for 2 days. Changes in any scaffold parameters seem unlikely, given that the majority of fatalities had nothing to do with the scaffold itself. We believe surgical procedures were consistent, and even more refined, so we believe that was not the problem. Although neither we nor the literature provides quantitative differences between trachea mechanical properties for rabbits at these ages, our team did note during the surgeries that the tracheas of the younger rabbits from this study felt more fragile during implantation than the older rabbits in our pilot studies, and thus for future studies for our group and others with trachea regeneration, we recommend using older (9 + lbs) rabbits, if not larger animal models.

It is suspected that the organic solvents used in electrospinning, if retained, could be cytotoxic *in vitro* or *in vivo*. *In vitro*, HFIP is toxic to chondrocytes at 500 ppm or higher.[26] Biopolymers (e.g., gelatin) have been shown to retain HFIP more than synthetic polymers (e.g., PCL), but the solvent content was significantly reduced (98%) by lyophilization and/or heating in a 50:50 gelatin/PCL blend scaffold.[26] Even though residual solvent can be reduced significantly, large scaffolds could contain a total solvent load that is toxic. Thus, researchers should consider evaluating residual solvent content with techniques like electrospray mass spectrometry, especially for larger animal studies or clinical use. For more efficient solvent removal, new techniques could be developed such as using higher vacuum, liquid-liquid extraction, or steam stripping, although these techniques would need to be customized to polymer and solvent properties.

The animal model for this study, the rabbit, was chosen because the trachea is similar in size to a pediatric trachea. After seeing this variable response to stenosis and delicate nature of the rabbit trachea, this leads us to reassess our animal model. There is no agreed upon animal model for tracheal research, and the animals have ranged from nude mice to pigs.[27] Recently, it was determined that the rabbit trachea has a reduced capacity to resist compressive or tensile forces compared with a sheep or human trachea.[28] While species selection is crucial, gender consideration should also be addressed by including male and female animals in future study designs. Per an NIH announcement, accounting for gender differences strengthens preclinical studies.[29] The male rabbit was an adequate model for small animal work, but future *in vivo* work should be gender inclusive and have a more mechanically robust trachea (e.g., sheep or pig).

Future directions and improvements for this work include measuring the stenosis during bronchoscopy (e.g., with a balloon or other method) to enable calculation of a percent reduction in area of a finite segment of the tracheal cylinder

encompassing the stenosis site. Additionally, evaluation of the added airway resistance of stenosis compared to the normal resistance would provide further data on scaffold performance. Further histological and immunohistological staining to clarify the specific immune cells types, for example, determining the type of macrophages (e.g., M1 vs. M2 polarization), which could illuminate the direction of healing.[30] In addition, a different surgical technique could be used to induce defects (e.g., laser or brush stenosis), to implant scaffolds (e.g., in line with trachea rather than overlap), and to revascularize (i.e., pedicle flap over implant). Most importantly, the scaffold could be redesigned to anchor the tracheal walls and prevent any wall migration into the airway. Success has been seen in extratracheal splints.[31] And finally, an autologous cell source should be used to cell-seeded group to ensure no adverse inflammatory response to allogenic cell sources.

In summary, we have illustrated that our scaffolds maintained functional airways in a majority of cases. Though the reasons that precipitated fatality are not readily apparent, evaluation of this scaffold in a larger animal model may ensure better outcomes given a more robust native trachea and the lack of failure noted with the scaffolds themselves. Other contingency plans for the larger animal model include improved implantation methods, redesign of a more mechanically robust scaffold, and potentially even epithelial cell seeding may ensure better outcomes. While the cell-seeded group had an improved survival rate, the Scaffold-only group had a higher occurrence of more patent airways and the BMSC group had reduced average cross-sectional areas. The BMSC group had a more severe accumulation of inflammatory cells over the graft, while also exhibiting more normal epithelium, subepithelium, and cartilage formation. This leads us to conclude that a simple, acellular scaffold is a viable option for tracheal tissue engineering, with the intraoperative addition of cells being an optional variation to the scaffolds. In conjunction with work to investigate reasons for tracheal obstruction disease pathology and development preventative treatment, our approach could treat patients who have already developed narrowing.

This was the first demonstration of an off-the-shelf fibrous gradient scaffold for patch-type tracheal defects with investigation of adding a growth factor or cells to the tracheal scaffolds. Our fibrous gradient scaffolds provide a potentially clinically relevant, off-the-shelf approach to tracheal defect repair.

Acknowledgments

We gratefully acknowledge support from the NSF CAREER Award (0847759), NIGMS Predoctoral Training Grant (T32 GM008359), and the Kansas Bioscience Authority Rising Star Award (M.S.D.). A special thanks to KU Medical Center Lab Animal Resources and Dr. Travis Hagedorn for their veterinary support.

Disclosure Statement

No competing financial interests exist.

References

1. Nouraei, S.A., Ma, E., Patel, A., Howard, D.J., and Sandhu, G.S. Estimating the population incidence of adult post-intubation laryngotracheal stenosis. Clin Otolaryngol **32,** 411, 2007.
2. Zias, N., Chroneou, A., Tabba, M.K., Gonzalez, A.V., Gray, A.W., Lamb, C.R., Riker, D.R., and Beamis, J.F., Jr. Post tracheostomy and post intubation tracheal stenosis: report of 31 cases and review of the literature. BMC Pulm Med **8,** 18, 2008.
3. Ott, L.M., Weatherly, R.A., and Detamore, M.S. Overview of tracheal tissue engineering: clinical need drives the laboratory approach. Ann Biomed Eng **39,** 2091, 2011.
4. Macchiarini, P., Jungebluth, P., Go, T., Asnaghi, M.A., Rees, L.E., Cogan, T.A., Dodson, A., Martorell, J., Bellini, S., Parnigotto, P.P., Dickinson, S.C., Hollander, A.P., Mantero, S., Conconi, M.T., and Birchall, M.A. Clinical transplantation of a tissue-engineered airway. Lancet **372,** 2023, 2008.
5. Steinke, M., Dally, I., Friedel, G., Walles, H., and Walles, T. Host-integration of a tissue-engineered airway patch: two-year follow-up in a single patient. Tissue Eng Part A **21,** 573, 2015.
6. Omori, K., Nakamura, T., Kanemaru, S., Asato, R., Yamashita, M., Tanaka, S., Magrufov, A., Ito, J., and Shimizu, Y. Regenerative medicine of the trachea: the first human case. Ann Otol Rhinol Laryngol **114,** 429, 2005.
7. Jungebluth, P., Alici, E., Baiguera, S., Le Blanc, K., Blomberg, P., Bozoky, B., Crowley, C., Einarsson, O., Grinnemo, K.H., Gudbjartsson, T., Le Guyader, S., Henriksson, G., Hermanson, O., Juto, J.E., Leidner, B., Lilja, T., Liska, J., Luedde, T., Lundin, V., Moll, G., Nilsson, B., Roderburg, C., Stromblad, S., Sutlu, T., Teixeira, A.I., Watz, E., Seifalian, A., and Macchiarini, P. Tracheobronchial transplantation with a stem-cell-seeded bioartificial nanocomposite: a proof-of-concept study. Lancet **378,** 1997, 2011.
8. Delaere, P., Vranckx, J., Verleden, G., De Leyn, P., and Van Raemdonck, D. Tracheal allotransplantation after withdrawal of immunosuppressive therapy. N Engl J Med **362,** 138, 2010.
9. Del Gaudio, C., Baiguera, S., Ajalloueian, F., Bianco, A., and Macchiarini, P. Are synthetic scaffolds suitable for the development of clinical tissue-engineered tubular organs? J Biomed Mater Res A **102,** 2427, 2014.
10. Naito, H., Tojo, T., Kimura, M., Dohi, Y., Zimmermann, W.H., Eschenhagen, T., and Taniguchi, S. Engineering bioartificial tracheal tissue using hybrid fibroblast-mesenchymal stem cell cultures in collagen hydrogels. Interact Cardiovasc Thorac Surg **12,** 156, 2011.
11. Lin, C.H., Su, J.M., and Hsu, S.H. Evaluation of type II collagen scaffolds reinforced by poly(epsilon-caprolactone) as tissue-engineered trachea. Tissue Eng Part C Methods **14,** 69, 2008.
12. Lazebnik, M., Singh, M., Glatt, P., Friis, L.A., Berkland, C.J., and Detamore, M.S. Biomimetic method for combining the nucleus pulposus and annulus fibrosus for intervertebral disc tissue engineering. J Tissue Eng Regen Med **5,** e179, 2011.
13. Xie, L., Lin, A.S., Levenston, M.E., and Guldberg, R.E. Quantitative assessment of articular cartilage morphology via EPIC-microCT. Osteoarthritis Cartilage **17,** 313, 2009.
14. Song, B.Z., Donoff, R.B., Tsuji, T., Todd, R., Gallagher, G.T., and Wong, D.T. Identification of rabbit eosinophils and heterophils in cutaneous healing wounds. Histochem J **25,** 762, 1993.
15. Kiesler, K., Gugatschka, M., Sorantin, E., and Friedrich, G. Laryngo-tracheal profile: a new method for assessing laryngo-tracheal stenoses. Eur Arch Otorhinolaryngol **264,** 251, 2007.

16. Belsey, R. Resection and reconstruction of the intrathoracic trachea. Br J Surg **38,** 200, 1950.
17. Grillo, H.C. Tracheal replacement: a critical review. Ann Thorac Surg **73,** 1995, 2002.
18. McNally, A.K., and Anderson, J.M. Macrophage fusion and multinucleated giant cells of inflammation. Adv Exp Med Biol **713,** 97, 2011.
19. Seguin, A., Baccari, S., Holder-Espinasse, M., Bruneval, P., Carpentier, A., Taylor, D.A., and Martinod, E. Tracheal regeneration: evidence of bone marrow mesenchymal stem cell involvement. J Thorac Cardiovasc Surg **145,** 1297, 2013.
20. Roberts, A.B., Sporn, M.B., Assoian, R.K., Smith, J.M., Roche, N.S., Wakefield, L.M., Heine, U.I., Liotta, L.A., Falanga, V., Kehrl, J.H., *et al.* Transforming growth factor type beta: rapid induction of fibrosis and angiogenesis in vivo and stimulation of collagen formation in vitro. Proc Natl Acad Sci U S A **83,** 4167, 1986.
21. Harrington, J.K., Chahboune, H., Criscione, J.M., Li, A.Y., Hibino, N., Yi, T., Villalona, G.A., Kobsa, S., Meijas, D., Duncan, D.R., Devine, L., Papademetri, X., Shin'oka, T., Fahmy, T.M., and Breuer, C.K. Determining the fate of seeded cells in venous tissue-engineered vascular grafts using serial MRI. FASEB J **25,** 4150, 2011.
22. Dormer, N.H., Gupta, V., Scurto, A.M., Berkland, C.J., and Detamore, M.S. Effect of different sintering methods on bioactivity and release of proteins from PLGA microspheres. Mater Sci Eng C Mater Biol Appl **33,** 4343, 2013.
23. Vadala, G., Mozetic, P., Rainer, A., Centola, M., Loppini, M., Trombetta, M., and Denaro, V. Bioactive electrospun scaffold for annulus fibrosus repair and regeneration. Eur Spine J **21 Suppl 1,** S20, 2012.
24. Li, L., Zhou, G., Wang, Y., Yang, G., Ding, S., and Zhou, S. Controlled dual delivery of BMP-2 and dexamethasone by nanoparticle-embedded electrospun nanofibers for the efficient repair of critical-sized rat calvarial defect. Biomaterials **37,** 218, 2015.
25. Ji, W., Sun, Y., Yang, F., van den Beucken, J.J., Fan, M., Chen, Z., and Jansen, J.A. Bioactive electrospun scaffolds delivering growth factors and genes for tissue engineering applications. Pharm Res **28,** 1259, 2011.
26. Nam, J., Huang, Y., Agarwal, S., and Lannutti, J. Materials selection and residual solvent retention in biodegradable electrospun fibers. J Appl Polym Sci **107,** 1547, 2008.
27. ten Hallers, E.J., Rakhorst, G., Marres, H.A., Jansen, J.A., van Kooten, T.G., Schutte, H.K., van Loon, J.P., van der Houwen, E.B., and Verkerke, G.J. Animal models for tracheal research. Biomaterials **25,** 1533, 2004.
28. Jones, M.C., Rueggeberg, F.A., Faircloth, H.A., Cunningham, A.J., Bush, C.M., Prosser, J.D., Waller, J.L., Postma, G.N., and Weinberger, P.M. Defining the biomechanical properties of the rabbit trachea. Laryngoscope **124,** 2352, 2014.
29. Clayton, J.A., and Collins, F.S. Policy: NIH to balance sex in cell and animal studies. Nature **509,** 282, 2014.
30. Brown, B.N., and Badylak, S.F. Expanded applications, shifting paradigms and an improved understanding of host-biomaterial interactions. Acta Biomater **9,** 4948, 2013.
31. Zopf, D.A., Flanagan, C.L., Wheeler, M., Hollister, S.J., and Green, G.E. Treatment of severe porcine tracheomalacia with a 3-dimensionally printed, bioresorbable, external airway splint. JAMA Otolaryngol Head Neck Surg **140,** 66, 2014.

Address correspondence to:
Michael S. Detamore, PhD
Department of Chemical and Petroleum Engineering
University of Kansas
4163 Learned Hall
1530 W 15th Street
Lawrence, KS 66045

E-mail: detamore@ku.edu

Received: April 3, 2015
Accepted: June 11, 2015
Online Publication Date: July 21, 2015